Received: 22 May 2016 | Accepted: 28 November 2016

DOI: 10.1111/jace.14715

ORIGINAL ARTICLE

Journal of the American Ceramic Society

C–(N)–S–H and N–A–S–H gels: Compositions and solubility data at 25°C and 50°C

Lauren Gomez-Zamorano[1,2] | Magdalena Balonis[3,4] | Bartu Erdemli[2] | Narayanan Neithalath[5] | Gaurav Sant[2,6]

[1]Programa Doctoral en Ingeniería de Materiales, Facultad de Ingeniería Mecánica y Eléctrica, Universidad Autónoma de Nuevo León, San Nicolás de los Garza, México

[2]Laboratory for the Chemistry of Construction Materials (LC^2), Department of Civil and Environmental Engineering, University of California, Los Angeles, California

[3]Department of Materials Science and Engineering, University of California, Los Angeles, California

[4]Institute for Technology Advancement, University of California, Los Angeles, California

[5]School of Sustainable Engineering and the Built Environment, Arizona State University, Tempe, Arizona

[6]California Nanosystems Institute (CNSI), University of California, Los Angeles, California

Correspondence
Lauren Gomez-Zamorano, Programa Doctoral en Ingenieria de Materiales, Facultad de Ingenieria Mecanica y Electrica, Universidad Autonoma de Nuevo Leon, San Nicolas de los Garza, Mexico.
Email: lauren.gomezzm@uanl.edu.mx
and
Magdalena Balonis, Department of Materials Science and Engineering, University of California, Los Angeles, CA
Email: mbalonis@ucla.edu

Funding information
Consejo Nacional de Ciencia y Tecnología, Grant/Award Number: 220312, 248165, CN-14-55, CN-14-55; National Science Foundation, Grant/Award Number: 1066583, 1401533; Federal Highway Administration, Grant/Award Number: DTFH61-13-H-00011.

Abstract

Calcium silicate hydrates containing sodium [C–(N)–S–H], and sodium aluminosilicate hydrates [N–A–S–H] are the dominant reaction products that are formed following reaction between a solid aluminosilicate precursor (eg, slags, fly ash, metakaolin) and an alkaline activation agent (eg NaOH) in the presence of water. To gain insights into the thermochemical properties of such compounds, C–(N)–S–H and N–A–S–H gels were synthesized with compositions: $0.8 \leq Ca/Si \leq 1.2$ for the former, and $0.25 \leq Al/Si \leq 0.50$ (atomic units) for the latter. The gels were characterized using thermogravimetric analysis (TGA), scanning electron microscopy with energy-dispersive X-ray microanalysis (SEM-EDS), and X-ray diffraction (XRD). The solubility products (K_{S0}) of the gels were established at 25°C and 50°C. Self-consistent solubility data of this nature are key inputs required for calculation of mass and volume balances in alkali-activated binders (AABs), and to determine the impacts of the precursor chemistry on the hydrated phase distributions; in which, C–(N)–S–H and N–A–S–H compounds dominate the hydrated phase assemblages.

KEYWORDS
calcium silicate hydrate, cements, geopolymers, solubility, thermodynamics

1 | INTRODUCTION

The alkali-activation of aluminosilicate minerals and industrial by-products has been a topic of considerable study over the past three decades.[1,2] Such alkali-activated binders (AABs) are produced by a chemical reaction between an aluminosilicate precursor (solid) and an alkaline activator (solution) to form a hardened solid. AABs demonstrate engineering properties similar to those of ordinary portland cement (OPC) mixtures, and may even have a lower CO_2 footprint than their performance equivalent OPC-based formulations,[3-5] However, the properties of AABs vary significantly depending on the nature of solid precursors (eg fly ash, metakaolin, slags, etc.), their reactivity, and the activation agents used (eg NaOH or Na_2SiO_3), which in turn alters the balances of product phases formed in the hardened state.[6]

The main reaction products of AABs comprise C–S–H gels that often contain aluminum with $0.80 \leq Ca/Si \leq 1.20$,[7,8] and which have sorbed, or weakly bonded alkalis (eg Na or K, sourced from the activator) and/or N–A–S–H gels (where $0.1 \leq Al/Si \leq 0.5$).[5,9] While the former product dominates in Ca-rich systems, eg, formed using a slag precursor, the latter product forms in the case of Ca-deficient formulations, eg, those produced using fly ash or metakaolin as the precursors. Both products feature an amorphous structure.[10-12] While the structure and solubility of C–S–H phases has been studied in great detail, far fewer studies have evaluated C–(N)–S–H and N–A–S–H* gels.[13-21.]

Briefly, C–S–H gels consist of silicate tetrahedra that are organized in chains, where two silicate tetrahedra share two oxygen atoms with a Ca-atom, while a third silicate tetrahedron shares oxygens with the paired tetrahedra forming a so-called "Dreierketten" structure.[22,23] On the other hand, the N–A–S–H gels present a three-dimensional structure of aluminum tetrahedra[24] where the charge imbalance generated by the replacement of Si^{4+} with Al^{3+}, is compensated by alkali cations (eg Na^+ or K^+ to ensure *valence compensation*) that are incorporated into the gel structure.[25,26] In N–A–S–H structures, for $Al/Si \leq 1$ (atomic ratio), the ordering of aluminum is expected to follow Loewenstein's rule, ie, of aluminum avoidance.[24]

Recently, Myers et al.,[12,27] presented a thermodynamic model for the C–(N)–A–S–H gels which accounts for the incorporation of Al and Na species into their structure. This model describes C–(N)–A–S–H gels as a solid solution composed of tobermorite-like end-members with substitutions of tetrahedral Al and Na species permitted. Further, Myers et al.[27] also presented solubility data of the C–A–S–H gels, including the effects of temperature on solubility equilibria for Ca/Si=1 and $Al/Si \leq 0.15$. It is significant to note that other than these studies,[12,27] and the zeolite literature, little data are available of solubility constants of N–A–S–H gels. Such lack of solubility data prevents calculation of mass and volume balances of AABs. These missing data are needed to establish the links between composition, microstructure, and engineering properties of AABs. Therefore, this paper tabulates original thermodynamic data of the C–(N)–S–H and N–A–S–H gels that is needed to implement quantitative thermodynamic calculations so as to resolve such linkages.

*Standard cement chemistry notation is used. As per this notation, C=CaO, N=Na_2O, A=Al_2O_3, S=SiO_2, H=H_2O. The parenthesis placed around "N" in C–(N)–S–H indicates that sodium may either physically sorb to, or substitutionally incorporate into the gel structure via weak atomic bonds.

2 | EXPERIMENTAL PROCEDURE

2.1 | Gel synthesis

Synthetic C–(N)–S–H gels of Ca/Si=0.8, 1.0 and 1.2 (atomic ratio; see Table 1) were prepared by double decomposition of calcium nitrate with sodium silicate, as described by Chen et al.[28] and by García-Lodeiro et al.[21] A 0.1 M solution of $Na_2SiO_3.5H_2O$ (AR-grade) and 0.08, 0.10 and 0.12 M solutions of $Ca(NO_3)_2$ (AR-grade) were prepared using Milli-Q water (resistivity of 18 MΩ·cm at 25°C). In a N_2-atmoshere, 100 mL of $Ca(NO_3)_2$ solution was added drop-by-drop to 100 mL of $Na_2SiO_3.5H_2O$ and 10 mL of 10 M NaOH solution. Stirring was continued for 7 days in air-tight plastic containers.

N–A–S–H gels with Al/Si=0.5 and 1.0 (atomic ratio; Table 1) were prepared using a procedure similar to that above. In a N_2-atmosphere, 50 mL of a 0.1 M $Al(NO_3)_2$ solution was added drop-by-drop to 100 mL of $Na_2SiO_3{\cdot}5H_2O$ and 10 mL of 10 M NaOH solution in an ice-bath while stirring.[29] Stirring was continued for 7 days in air-tight plastic containers.

Syntheses of both gel families was carried out from under-saturation (see compositions in Table 1). Following precipitation, both the C–(N)–S–H and N–A–S–H gels were washed using 2 L of Milli-Q water and vacuum filtered in a N_2 atmosphere.[26] The samples were subsequently dried at room temperature, for 15 days using $CaCl_2$ as a desiccant. Once dry, the gels were ground using an agate mortar and pestle, prior to further analyses.

2.2 | Characterization

A Perkin Elmer (Waltham, MA, USA) STA 6000 simultaneous thermal analyzer (TGA/DTG/DTA) with a Pyris data acquisition interface was used to characterize the gels. The powder samples were heated under ultrahigh purity N_2 purge at a heating rate of 10°C/min over a temperature range from 35-to-975°C. During the heating step, the

TABLE 1 The chemical formulas of the synthesized C–(N)–S–H and N–A–S–H gels.

	Target composition (atomic ratio)	Identifier	Chemical formula (normalized per mole of SiO_2)
Ca/Si	0.80	C–(N)–S–H 0.8	$(CaO)_{0.74}\cdot(Na_2O)_{0.08}\cdot(SiO_2)_1\cdot(H_2O)_{1.89}$
	1.00	C–(N)–S–H 1.0	$(CaO)_{0.97}\cdot(Na_2O)_{0.12}\cdot(SiO_2)_1\cdot(H_2O)_{2.09}$
	1.20	C–(N)–S–H 1.2	$(CaO)_{1.16}\cdot(Na_2O)_{0.17}\cdot(SiO_2)_1\cdot(H_2O)_{2.17}$
Al/Si	1.00	N–A–S–H 1	$(Na_2O)_{0.45}\cdot(Al_2O_3)_{0.45}\cdot(SiO_2)_1\cdot(H_2O)_{2.48}$
	0.50	N–A–S–H 2	$(Na_2O)_{0.26}\cdot(Al_2O_3)_{0.24}\cdot(SiO_2)_1\cdot(H_2O)_{1.88}$

samples were first equilibrated at 40°C for 60 minutes to gently remove excess water, and then heated up to 975°C. The mass loss (TGA) and differential weight loss (DTG) patterns acquired were used to identify thermal decomposition behavior.

Qualitative X-ray diffraction (XRD) analyses were carried out on the powdered gels using a Bruker D8 (Bruker Corporation, Billerica, MA, USA) Advance diffractometer using Cu$K\alpha$ radiation (λ=1.54 Å). The samples were scanned on a rotating stage between 5-and-70° (2θ); with a step scan of 0.021° and a dwell time of 1 second. The time required for acquisition of a X-ray diffraction pattern was around 50 minutes. X-ray structure data for known compounds were sourced from the literature or standard databases (ICSD, JCPDS).[30]

The density of the solid gels was analyzed using a Micromeritics (Micromeritics Corporation, Norcross, GA, USA) AccuPyc II Pycnometer. This technique uses a gas (Helium) displacement method to measure the solid volume, and hence density accurately.

The morphology of the gels and their atomic compositions were studied by scanning electron microscopy (SEM). Samples were prepared by dispersing the gel powders onto double-sided adhesive carbon tape held on an aluminum stub. The gels were sputter-coated with a gold film to reduce charging. The compositions of the gels were determined by X-ray microanalysis (EDS) using a fast-EDS detector (ie, to mitigate issues of mobility of light elements under electron-beam irradiation) as averaged over 50 discrete points. To avoid any inconsistences in the analyses,[31] the same operational parameters were used, eg, the working distance (5 mm), spot size (4.5), accelerating voltage (15 kV), and a dead time between 15-to-25%. The SEM-EDS data and thermal analysis results were combined to assess the total and the nonevaporable water contents of the gels using the formula noted below (Equation 1):

$$H_2O = \frac{TW\left(\frac{Na_2O}{2}\cdot MW_{Na_2O} + CaO\cdot MW_{CaO} + SiO_2\cdot MW_{SiO_2} + \frac{Al_2O_3}{2}\cdot MW_{Al_2O_3}\right)}{(100-TW)MW_{H_2O}} \quad (1)$$

where: H_2O is the water content in a given gel (moles); TW is the total water content (sum of evaporable and nonevaporable water), that is the mass of water lost (g) between 40°C-to-975°C,[32] and Na_2O, CaO, SiO_2, and Al_2O_3 are the average quantities of these oxides in the gels (moles) as determined via SEM-EDS analyses and MW is the molar mass of each simple oxide (g/mole). The inter-sample variability (standard deviation) in the molar water content calculated in this manner is on the order of 2%.

Solubility data of the gels were determined by dispersing 1 g of each powder in 30 mL of MilliQ water (EMD Millipore Corporation, Temecula, CA, USA) contained in air-tight PTFE bottles. These samples were maintained at 25°C and 50°C in shaking incubators for 90 days. After equilibration, the solutions were filtered through syringes fitted with a 0.22 μm filter, and acidified with HNO_3 (15.8 N) to stabilize the solution. To avoid carbonation, the preparatory process was carried out within a glove-box in a N_2-atmosphere. The concentrations of Ca, Si, Na and Al obtained for six different solutions prepared using solids from the same synthesis batch were analyzed by inductively coupled plasma-optical emission spectroscopy (ICP-OES) using a Thermo iCAP6300 (Thermo Fisher Scientific, Waltham, MA, USA). The measured solution concentrations were used to calculate solubility constants (K_{S0}, unitless) of the gels using the GEMS-PSI software (see Section 5). The solution compositions are noted in the supplementary information (SI).

3 | RESULTS AND DISCUSSION

Figures 1-2 show the results of EDS analysis of both the C–(N)–S–H and N–A–S–H gels. Secondary electron images (see Figure S1 and S2 from SI) illustrate the globular morphology of C–(N)–S–H and N–A–S–H gels.[26,33] There is little if any difference in the "visual appearance" of the two gels, and no evidence of any calcium or sodium carbonate solids (ie, with a well-defined, plate-like morphology) was found.

For the C–(N)–S–H gels, the EDS results of the Na/Ca vs Si/Ca plot (Figure 1A), indicates a chemical composition that is dominant in Ca and Si, but with small amounts of Na that persist; likely from the synthesis process. The measured Ca/Si ratio was slightly lower than the target

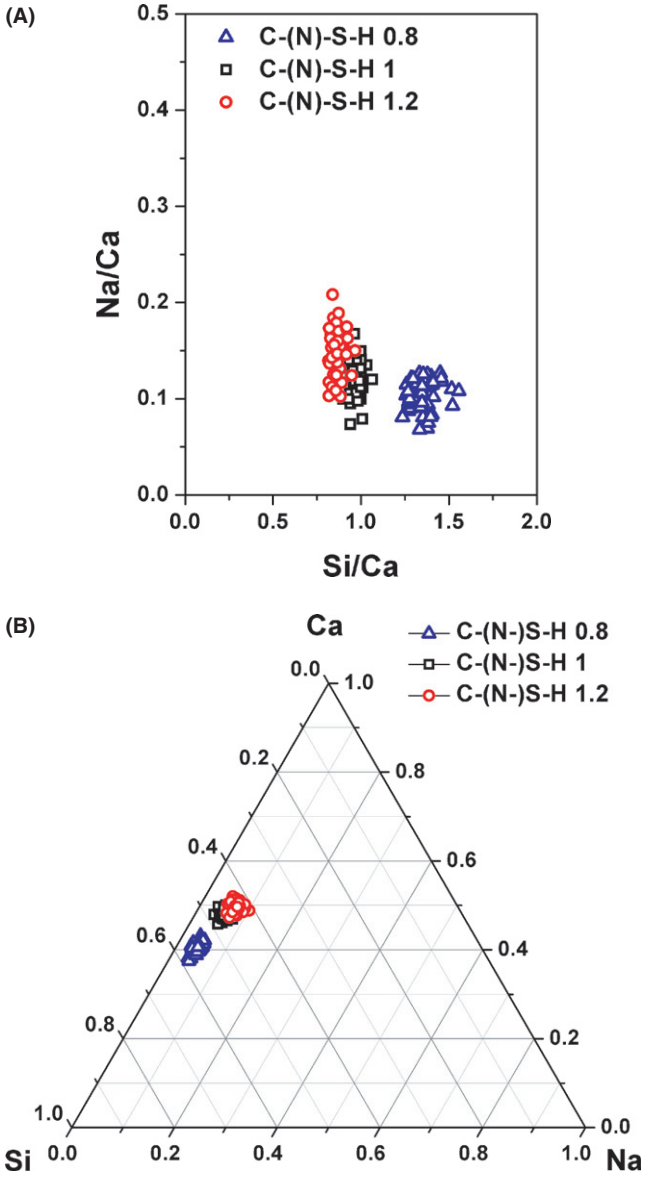

FIGURE 1 (A, B) The atomic compositions of the C–(N)–S–H gels as determined by SEM-EDS analysis [Color figure can be viewed at wileyonlinelibrary.com]

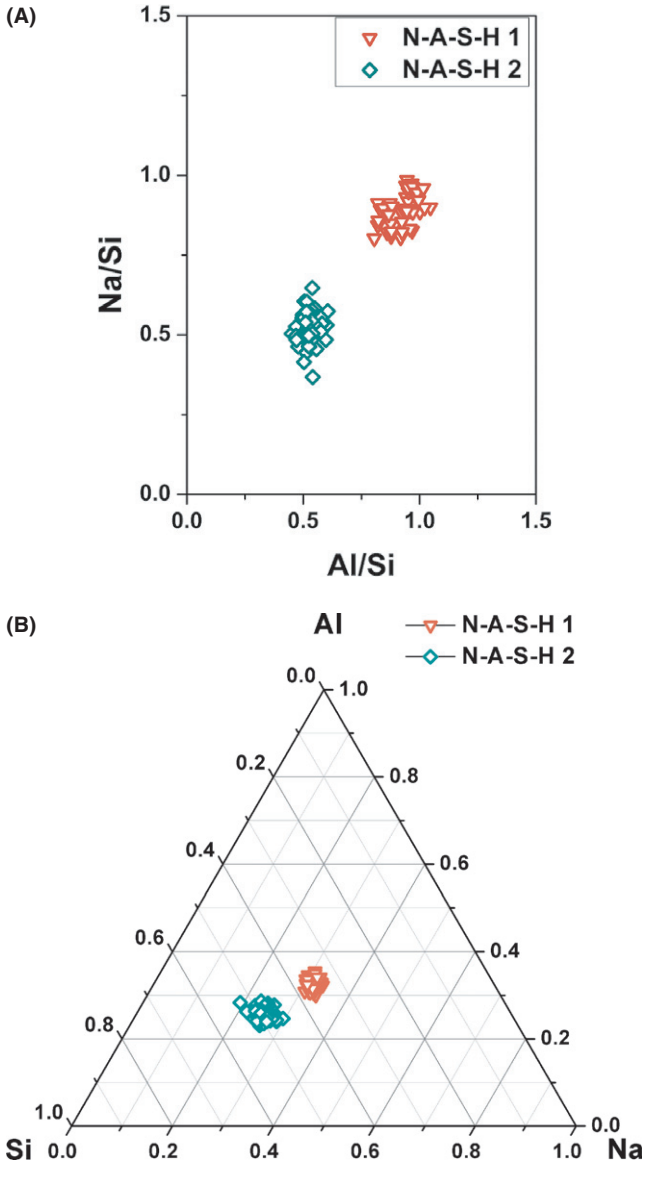

FIGURE 2 (A, B) The atomic compositions of the N–A–S–H gels as determined by SEM-EDS analysis [Color figure can be viewed at wileyonlinelibrary.com]

value (within 8% or less, see Table 1), likely due to the presence of alkalis during synthesis.[34,35] It has been reported that during C–S–H formation, its structure and composition are affected by the presence of alkalis, eg, which may physically sorb onto the gel surfaces, or may be weakly bonded to the C–S–H structure.[36] Such weak bonding or sorption of alkalis (eg, Na or K) on the C–S–H gel is a function of Ca/Si ratio.[18,34,37] For example, in alkali-activated slags, Na can insert itself into the gel structure (eg, see[38]), by partially occupying Ca-atom positions in the C–S–H/C–(N)–S–H gels – an effect which enhances with reducing Ca/Si. Alternately, Garcia-Lodeiro suggested that an alternate gel that incorporates Na-species in its structure could also form (eg, in a region of a miscibility gap), besides the more typical case of Ca-substitution, or Na-sorption on the gel surfaces[26], but further study is needed to better clarify such aspects.

In the case of N–A–S–H gels, the average Al/Si ratio obtained was slightly higher than the design value (Table 1 and Figure 2; within ±10%), since N–A–S–H gels form heterogeneously.[2,39] More specifically, two precursor gels form, Gel 1 which is initially rich in aluminum, and Gel 2 which is rich in silicon. The intermixing of the two gels locally is postulated to induce variations from the bulk composition across sampling points. It should be noted, however, that the bulk compositions of gels formed (see Figure 2) were in agreement with compositions suggested in the literature.[26,40,41] The source of soluble silica used, and the nature of Si-species (eg, monomers, dimers, etc.)

present in the solution, strongly influences the reaction kinetics of gel formation and their composition.[6,41,42] For example, reductions in the molar SiO_2/Na_2O ratio hasten gelation rates as monomeric Si-species are increasingly mobilized at higher pH. This facilitates the formation of gels with lower Al/Si, as observed in Table 1.

Figure 3 shows thermal decomposition profiles of the N–A–S–H gels. These gels are emphasized over the C–(N)–S–H gels, as the latter have been extensively studied previously.[28,43] In brief, similar to C–S–H gels, N–A–S–H gels show continuous mass loss across the range of temperatures studied. The mass loss occurs on account of the removal of evaporable and nonevaporable water, of which the former dominates. Mass loss increases with Al/Si ratio, with the Al/Si=1.0 gel showing more mass loss than the Al/Si=0.5 gel. Little mass loss occurs beyond 500°C, and both portlandite and calcite are uniformly absent in the synthetic C–(N)–S–H gels.

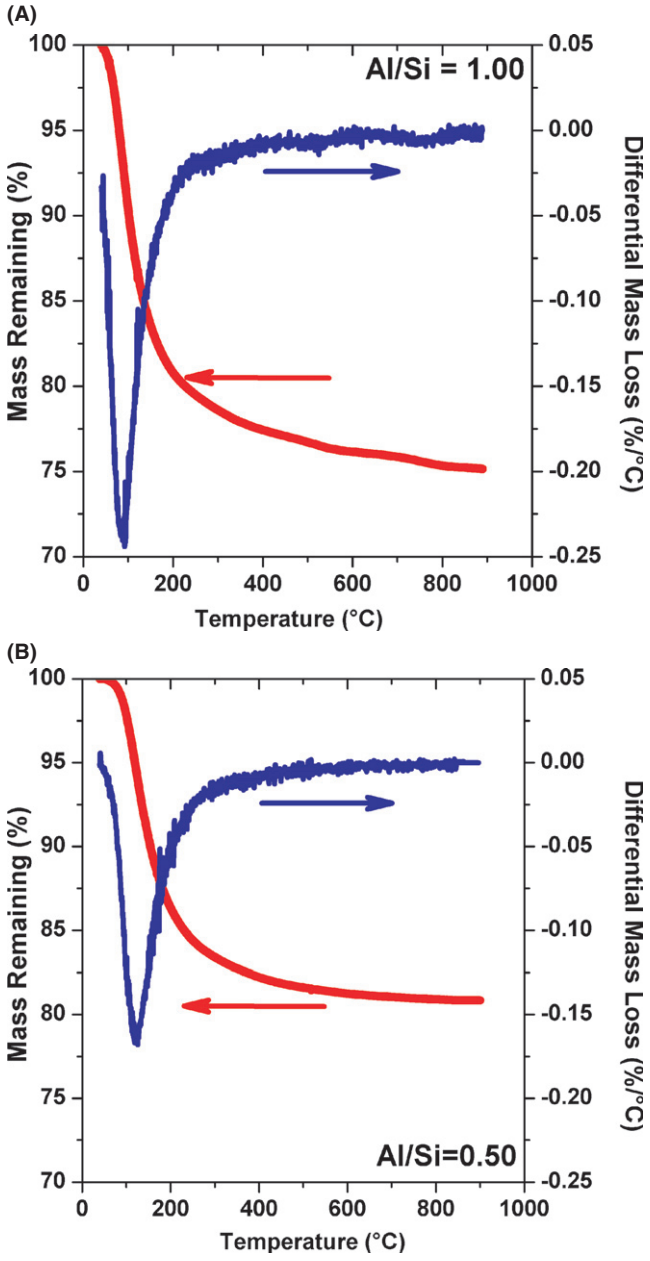

FIGURE 3 Thermogravimetric decomposition profiles of the N–A–S–H gels for: (A) Al/Si=1.00 and (B) Al/Si=0.50 (atomic ratio) [Color figure can be viewed at wileyonlinelibrary.com]

Figure S3 (in the SI) shows powder XRD reflections of the N–A–S–H and C–(N)–S–H gels. The XRD patterns for C–(N)–S–H gels show a distinct lack of calcium carbonate, and portlandite – a point that was also confirmed by calculations of saturation indices for these compounds using the measured solution data (eg, see Table S1, SI). As such, it is confirmed that the as-synthetized gels are free of any other impurities or contaminants. Furthermore, the C–(N)–S–H gels show a dominant X-ray reflection at a basal spacing of ≈1 nm, independent of Ca/Si ratio, from 0.8-to-1.2, as has been observed previously.[44]

The C–(N)–S–H gels show the same number of diffraction maxima at similar 2θ positions and intensities. Sharp X-ray reflections are noted at basal spacings of 0.31, 0.28, and 0.18 nm in agreement with Chen et al.[28] These observations suggest that the C–(N)–S–H gels are comparable to 11 Å tobermorite,[28] which shows basal reflections at similar positions. A weak X-ray reflection at 0.17 nm (that is un-attributed), and the presence of silica gel that is marked by a broad hump starting at around 22° (2θ) are also observed. The significant peak broadening observed compared to XRD patterns of tobermorite suggests the presence of distinct nanoscale domains in the gel.

For the N–A–S–H gels, their XRD patterns exhibit a broad hump around 20°-to-35° (2θ), indicating an amorphous phase that is similar to that observed in alkali activated fly ashes, and their fly ash precursors.[39,41] There is no evidence of any crystalline zeolitic or other impurities in the gel compositions, based on the absence of sharp, well-defined X-ray peaks.

4 | CORRELATING SOLID AND SOLUTION COMPOSITIONS OF THE C–(N)–S–H AND N–A–S–H GELS

Figure 4A shows the Ca/Si in the solid and liquid phases for C–(N)–S–H gels equilibrated at 25 and 50°C for 3 months. The trend is similar to those noted by Chen et al.[28,45] The observed trends imply that the gels are free of any Ca–OH bonds and the structures are based on 11 Å tobermorite, as confirmed by XRD analyses (Figure 4). Brown[46] noted that in the formation of Na-substituted C–S–H, a small content of Na_2O in C_3S greatly increased the pH and also decreased the Ca-content in the solid. Contrastingly, Kumar et al. noted that independent of the

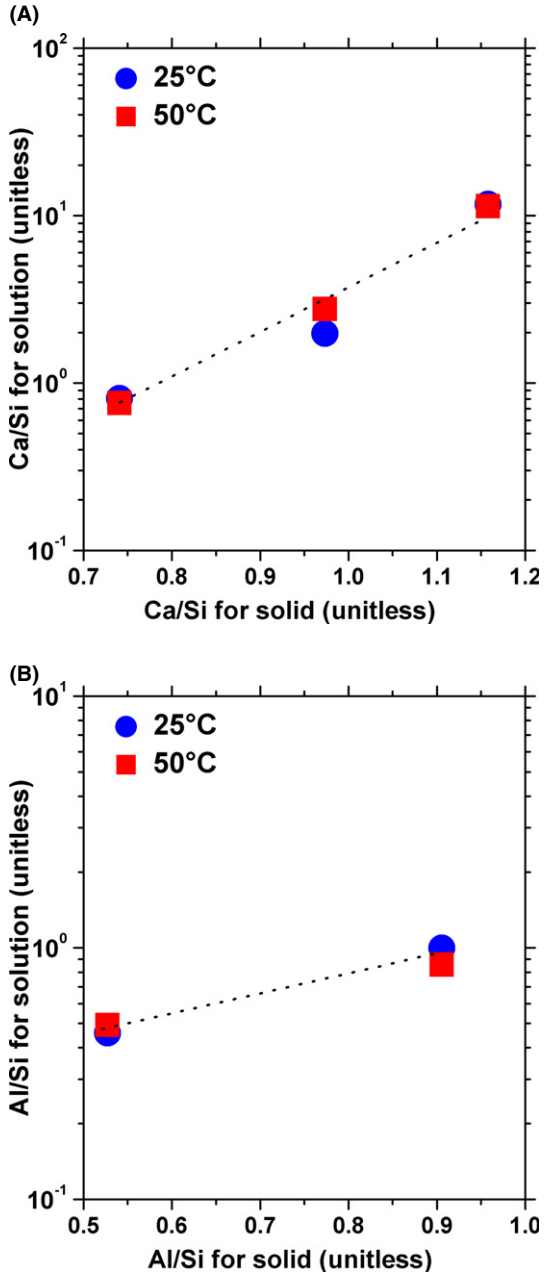

FIGURE 4 (A) Ca/Si in the solution as a function of Ca/Si in the solid for C–(N)–S–H gels and (B) Al/Si in the solution as a function of Al/Si in the solid, for N–A–S–H gels. The trends suggest that C–(N)–S–H dissolves incongruently for Ca/Si >0.80 (in the solid), while the dissolution of the N–A–S–H gels is congruent [Color figure can be viewed at wileyonlinelibrary.com]

addition of alkalis, the Ca/Si of C–S–H remained unchanged (ie, Ca/Si≈1.7), when the latter formed by the hydration of C_3S in water.[34] In the present gels, which formed in the presence of Na, the Na-content increases with Ca/Si ratio of the solids. On the other hand, in the case of previously synthesized C–S–H that was thereafter exposed to NaOH solutions, the extent of Na-uptake, reduces with Ca/Si.[37] This suggests that a common-ion effect likely controls the extent of Na-uptake during C–S–H synthesis. This may also explain why for redispersed C–(N)–S–H particulates the Ca-abundance in solution changes with Ca/Si of the solids as shown in Figure 4A (see also SI). For example, it is noted that, Ca/Si in the solid, and solution is equivalent only for Ca/Si≈0.80 (for solid). At higher Ca/Si levels in the solid, Ca/Si in solution is substantially higher, indicating that C–(N)–S–H dissolution is becoming increasingly incongruent as observed elsewhere.[28,47]

Unusually high aqueous Si and low Ca concentrations in C–(N)–S–H systems have been observed by Macphee et al.,[35] who noted that the precipitates were silica-rich. This may suggest that with increasing Ca/Si, the C–(N)–S–H gels solubilize by a leaching-type process wherein Ca is selectively, and preferentially removed. This would result in the residual compositions being Si-rich. To confirm this point, the C–(N)–S–H gels were removed from the solution after 3 months of equilibration, and reanalyzed by SEM-EDS. The results indicate that gels with Ca/Si≈0.80 at the time of synthesis maintain their original composition (ie, Ca/Si≈0.78 at both 25 and 50°C after equilibration in water for 3 months), but show a near complete lack of Na in the solid.

At higher Ca/Si ratios, Brown et al. and Macphee et al. noted that the residual solids were Si-rich,[35,46]; as would be expected based on the observations of Ca/Si in solution which indicates incongruent dissolution. Here, gels with Ca/Si≈1 showed Ca/Si≈2 (in solution), and gels with Ca/Si≈1.2 presented Ca/Si≈11 (in solution) following equilibration in water for 3 months. This suggests that an increase in solid Ca/Si, and Na-content increases the extent of incongruency of gel dissolution. The results also justify that Na in C–(N)–S–H gels is held by weak bonds, as its near complete removal suggests physisorption.[18,37] However, SEM-EDS analysis of the solids at the end of 3 months indicated that the gels were only slightly Ca-depleted. For example, gels with Ca/Si≈1.0 and 1.2 at the time of synthesis features Ca/Si≈0.93 and 1.08, respectively, at both 25 and 50°C; a change of ≤7%. Temperature is noted to have little if any impact on the results. While this conclusion differs from that of Glasser et al.,[48,49] who noted a reduction in Ca^{2+} concentration with temperature, they used a somewhat higher temperature (55°C), where some gel crystallization may have occurred over long equilibration periods. This was not the case for the gels studied here as XRD analysis of the solid wastes, only showed an amorphous halo around 20-30° 2θ (see Figure S4 form SI).

Figure 4B shows the measured Al/Si in the solid and liquid phases for N–A–S–H gels equilibrated at 25 and 50°C for 3 months. It has been reported[50] that in solutions near saturation with respect to a zeolite with Al/Si≈0.50, reactions among silicate and aluminosilicate species are

rapid. In spite of the amorphous nature of the present gels, the fast equilibration explains why Al/Si in the solid and solution are similar to each other – indicative of congruent dissolution across the entire range of compositions studied. It is also seen that the Al/Si ratios increase in proportion with gel composition. Temperature slightly, if at all, influences Al/Si ratios in the solution and the solid. It should be noted that the SEM-EDS analysis of the residual N–A–S–H gels at the end of the equilibration period showed a difference in composition of ≤4% (in terms of Al/Si). Furthermore, XRD patterns obtained at the end of solubility analyses were also similar to those obtained initially (see XRD patterns in Figure S4, SI). This too, supports the conclusion of congruency in dissolution.

According to Fernandez-Jimenez et al.,[39] both the curing temperature and the nature of the alkali ions present affect the kinetics of geopolymer formation. As such, while the reaction rate increases with curing temperature, different products may also form. They also reported that aluminum is rapidly consumed during N–A–S–H formation[39] with the behavior of such systems being similar to an Ostwald ripening process.[39] Further, it is anticipated that Na-taken up by the gel structure is located in close proximity to aluminum ions to balance the charge deficit that does result from the valence mismatch resulting from Si^{4+} for Al^{3+} substitutions.[39]

5 | CALCULATION OF SOLUBILITY CONSTANTS OF C–(N)–S–H AND N–A–S–H GELS

Equilibrium (solubility) constants were calculated using the solution compositions measured in Table 1 while assuming the reactions noted in Table 2. Given the presence of Na in the C–(N)–S–H gels, such species are explicitly identified in the dissolution reaction, as upon gel dispersion in water, Na is expected to exhaust into the solution from solids where its presence will influence ion equilibrium. All calculations were carried out using a geochemical speciation code, GEMS-PSI: Gibbs Energy Minimization Software, version 2.3 which includes a native GEM solver,[51] a built in NAGRA-PSI 'Kernel' and slop98.dat and CEMDATA07 thermodynamic databases (see SI for relevant thermodynamic data of aqueous species, Table S2),[52-54] including recent data from Myers et al.[55] The activity of any relevant ion in solution is described by the Truesdell-Jones modification of the extended Debye-Hückel equation as written in Equation (2):

$$\log \gamma_i = \frac{-Az_i^2\sqrt{I}}{1 + B\alpha_i\sqrt{I}} + bI \quad (2)$$

where, γ_i is the activity coefficient of any ion 'i' (unitless), A and B are Debye-Hűckel solvent parameters dependent on the dielectric constant of water and temperature (unitless), z_i is the ion valence, α_i is a parameter dependent on the ion size (ie, Kielland's parameter for individual ions,[53] unitless), 'b' is a semi-empirical parameter (0.0064 at 25°C) and I is the ionic strength (mol/L). The solubility constants that were calculated using the relevant ion activity products (IAP's) are tabulated in Table 3 and are shown in Figures 4-5, respectively.

The calculated solubility products can be used to determine the Gibbs free energy of reaction $\Delta_r G^0{}_T$ (kJ/mole), for a given dissolution reaction as noted in Equation (3a). Since solubility data were acquired at two different temperatures, ie, 25°C and 50°C, this data can be used to determine the temperature dependence of the solubility product using the Van't-Hoff relation (Equation 3b), which tabulates the enthalpy of the dissolution reaction (ΔH_r, kJ/mole):

$$\Delta_r G_T^0 = -RT\ln(K_{S0}(T)) \quad (3a)$$

$$\ln(K_{S0}(T)) = \ln(K_{S0}(T_R)) + \frac{\Delta H_r}{R}\left(\frac{1}{T_R} - \frac{1}{T}\right) \quad (3b)$$

where, R is the ideal gas constant (8.315 J/K.mole), T is the thermodynamic temperature, and T_R is the reference temperature, taken as 298.15 K. It should be noted, ideally, application of the Van't-Hoff or any other method of establishing temperature dependence requires observations of a property for at least three different temperatures. While this condition is not satisfied herein, since only two temperature are considered, it is expected that this limitation is most

TABLE 2 The dissolution reactions used to calculate solubility products for a given phase

Phase ID	Dissolution reactions
C–(N)–S–H 0.8	$(Na_2O)_{0.078}(CaO)_{0.74}(SiO_2)_1(H_2O)_{1.89}$=0.156 Na^++0.74 Ca^{2+} + 1 $HSiO_3^-$+0.636 OH^-+1.072 H_2O
C–(N)–S–H 1.0	$(Na_2O)_{0.122}(CaO)_{0.973}(SiO_2)_1(H_2O)_{2.09}$=0.244 Na^++0.973 Ca^{2+}+1 $HSiO_3^-$+1.19 OH^-+0.995 H_2O
C–(N)–S–H 1.2	$(Na_2O)_{0.173}(CaO)_{1.158}(SiO_2)_1(H_2O)_{2.17}$=0.346 Na^++1.158 Ca^{2+}+1 $HSiO_3^-$+1.662 OH^-+0.839 H_2O
N–A–S–H 1	$(Na_2O)_{0.45}(Al_2O_3)_{0.45}(SiO_2)_1(H_2O)_{2.48}$=0.9 Na^++0.9 AlO_2^-+1 $SiO_2{}^0$+2.48 H_2O
N–A–S–H 2	$(Na_2O)_{0.26}(Al_2O_3)_{0.24}(SiO_2)_1(H_2O)_{1.88}$=0.52 Na^++0.48 AlO_2^-+0.96 $SiO_2{}^0$+0.04 $HSiO_3^-$+1.84 H_2O

TABLE 3 Solubility constants, standard molar Gibbs free energies of formation and the density of C (N)–S–H and N–A–S–H phases at T=25°C and p=1 bar

Phase ID	Composition	log K_{S0}	$\Delta_f G^0$ (kJ/mole)	ρ (g/cm^3)
C–(N)–S–H 0.8	$(Na_2O)_{0.078}(CaO)_{0.740}(SiO_2)_1(H_2O)_{1.89}$	−7.77	−1862.90	2.18
C–(N)–S–H 1.0	$(Na_2O)_{0.122}(CaO)_{0.973}(SiO_2)_1(H_2O)_{2.09}$	−9.99	−2096.54	2.22
C–(N)–S–H 1.2	$(Na_2O)_{0.173}(CaO)_{1.158}(SiO_2)_1(H_2O)_{2.17}$	−12.05	−2274.52	2.34
N–A–S–H 1	$(Na_2O)_{0.45}(Al_2O_3)_{0.45}(SiO_2)_1(H_2O)_{2.48}$	−9.05	−2453.72	1.78
N–A–S–H 2	$(Na_2O)_{0.26}(Al_2O_3)_{0.24}(SiO_2)_1(H2O)_{1.88}$	−6.58	−1848.00	1.94

impactful for temperatures below 10°C and above 70°C – as broadly, solubility relations for intermediate temperatures follow near linear correlations. According to Damidot, et al,[56] over a narrow temperature interval (such as 25°C-to-50°C), good agreement was observed between the Van't Hoff equation and the three-term approximation. It should also be noted that rather than a three-term temperature extrapolation,[57] the linear Van't-Hoff approach is chosen for fitting the temperature-dependent K_{S0} as entropy and heat capacity data, especially for N–A–S–H gels, is not available at this time.

Figures 5 and 6 show the solubility data of the C–(N)–S–H and N–A–S–H gels as a function of their composition (ie, Ca/Si or Al/Si) and temperature. It is noted that across all compositions and gel types, the solubility constants decrease, taking more negative values with an increase in the Ca/Si or Al/Si. It should be noted that while the current tabulations of K_{S0} for C–(N)–S–H gels do consider Na in the dissolution reaction, disregarding Na has little effect on K_{S0}. The uncertainty in the calculated K_{S0} is on the order of 0.25 log units, due to uncertainties stemming from the ion concentration measurements. In general, C–(N)–S–H gels are less influenced by temperature than their N–A–S–H counterparts (see Figure 4). This suggests that temperature would only very slightly influence mass and volume balances of C–(N)–S–H gels, across the range of temperatures studied. Over the temperature range of interest, the structure of the C–(N)–S–H gels remains disordered, and no changes in atomic packing density, or the water content occur.

The solubility trends are inverted across the two gel types, eg, while C–(N)–S–H gels become less soluble with increasing temperature (K_{S0} becomes more negative), N–A–S–H gels become more soluble with increasing temperature, with their K_{S0} taking less negative values.

These trends are clearly borne out in Figure 6 which highlights that while dissolution of the C–(N)–S–H gels is exothermic, albeit to different levels, the N–A–S–H compositions demonstrate endothermic dissolution. Also, while the N–A–S–H compositions show near-equivalent enthalpies of dissolution, the C–(N)–S–H gels show an inversion in dissolution enthalpy around Ca/Si≈1.0 (see Figure 6C). This suggests that the structure of the C–(N)–S–H gels undergoes a change across the Ca/Si≈1.0 boundary, as suggested by Alizadeh.[44] The present tabulations of K_{S0} for the C–(N)–S–H gels are in agreement with literature data for pure C–S–H,[58,59] compositions (see Figure 7). This suggests the negligible relevance of sodium in altering solubility equilibria.

Clear comparisons of N–A–S–H solubility equilibria are more difficult as the only comparisons for similar compositions are to zeolites (eg, zeolite for Al/Si=1.0 (see ref[50]), which show a well-ordered crystalline structure, and whose solubilities have been measured only at temperatures, ranging between 353 K-to-363 K.[50] It should be highlighted that both Ca-rich and Na-rich gel families show similar solubility constants, in terms of their numerical values. Given the similar structural role of silicon in both compositions, it is possible that if these gels were to form by co-precipitation, one of the gel families may dominate the other; in terms of mass abundance. Thus, only upon the exhaustion of species (in terms of ion activities, rather than concentration) requisite for formation of one of the gels (eg Ca, for C–(N)–S–H) would the other gel form (ie, N–A–S–H) readily. Such an idea was also put forth by Garcia-Lodeiro et al.,[21,25,29] – who noted that Ca-rich gels would be preferred in comparison to their Na-rich counterparts. This would exert controls on the time-dependent (ie, kinetic) evolution of phase balances, and the time-dependent evolution of engineering properties in AAB formulations.

6 | CONCLUSIONS

A series of synthetic C–(N)–S–H and N–A–S–H gels were produced by a double decomposition method to analyze their compositions and solubility products. The XRD patterns of the N–A–S–H showed a broad halo previously reported for amorphous aluminosilicates and no evidence of any zeolite-like (crystalline) phases was found. For C–(N)–S–H gels, the XRD results indicated a low degree of ordering in the three different gel compositions, which showed peaks similar to those of 11 Å

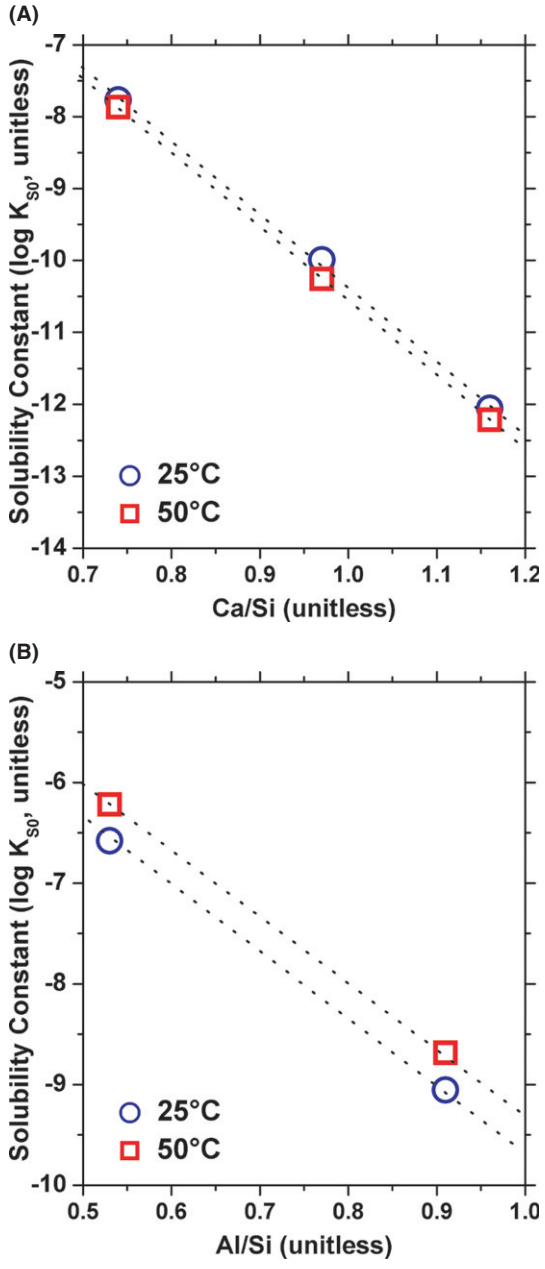

FIGURE 5 The equilibrium solubility constant (K_{S0}) of: (A) C–(N)–S–H gels as a function of measured Ca/Si (atomic ratio) of the solids and (B) N–A–S–H gels as a function of measured Al/Si (atomic ratio) of the solids. The uncertainty in the measured solubility constants is on the order of ±0.25 log units (based on the uncertainty in solution compositions) [Color figure can be viewed at wileyonlinelibrary.com]

tobermorite. The gel compositions were examined via SEM-EDS analyses and the water content estimated by thermal analyses.

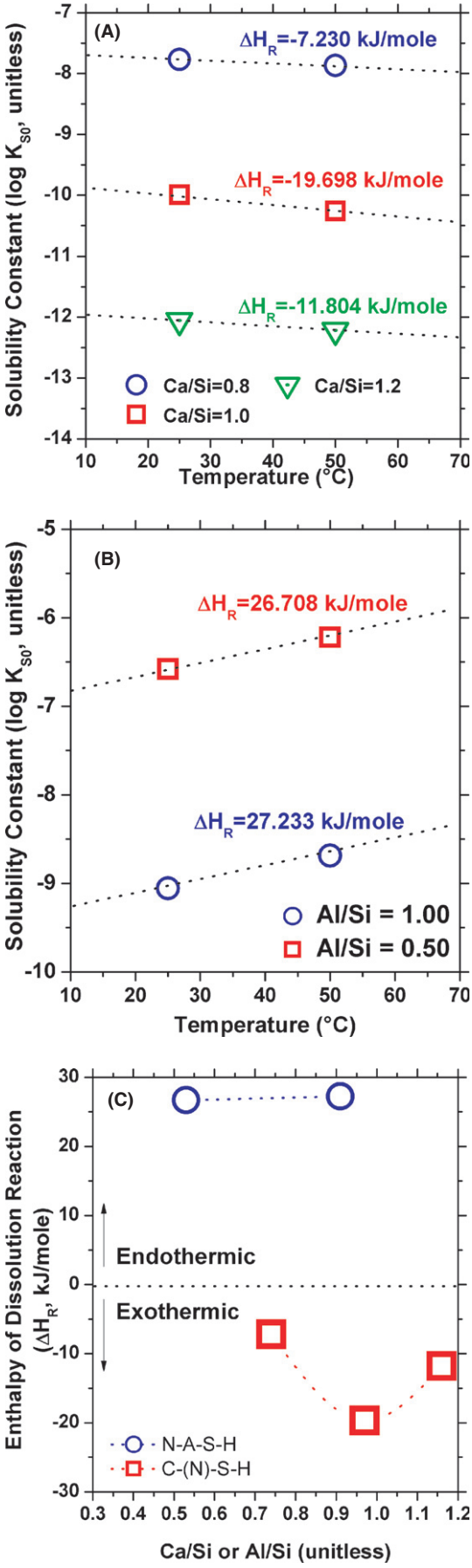

FIGURE 6 The equilibrium solubility constant (K_{S0}) of: (A) C–(N)–S–H gels as a function of temperature and (B) N–A–S–H gels as a function of temperature. (C) The enthalpy of dissolution as a function of the measured Ca/Si or Al/Si (atomic ratio) of the solid phase [Color figure can be viewed at wileyonlinelibrary.com]

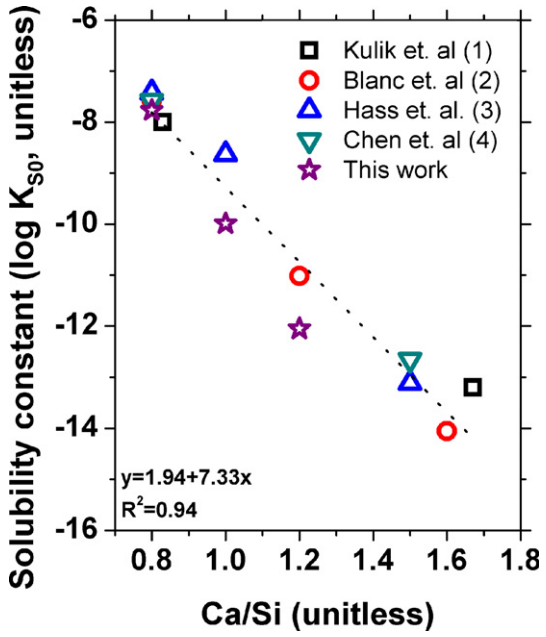

FIGURE 7 Comparison of the 25°C equilibrium constants of synthetic C–(N)–S–H gels and using data from: (1) Kulik et al.,[56] (2) Blanc et al.[42] (3) Hass et al.,[57] and (4) Chen et al.[27] [Color figure can be viewed at wileyonlinelibrary.com]

The concentrations of Ca and Si species in the aqueous phase, equilibrated with the solid gels, followed expected patterns with C–(N)–S–H showing increasing incongruency in dissolution with increasing Ca/Si, and the Na-content of the gels. For N–A–S–H gels, the solids and aqueous phase showed equivalent Al/Si ratios, indicative of congruency in dissolution across the entire range of compositions studied. In general, the solubility increased with temperature for N–A–S–H gels and decreased for C–(N–)–S–H gels. Original data of the solubility constants (K_{S0}), density, Gibbs free energies of formation, and enthalpy of dissolution for these gel families that is tabulated herein provides critical inputs needed for calculation of mass and volume balances in AAB systems.

ACKNOWLEDGMENTS

The authors acknowledge financial support for this research provided by: the National Council of Science and Technology (CONACYT-Mexico), UC-Mexus Program of the University of California and CONACYT-Mexico, Universidad Autónoma de Nuevo León (UANL), U.S. National Science Foundation (CMMI: 1066583, 1401533) and the Federal Highway Administration (DTFH61-13-H-00011). The contents of this paper reflect the views of the authors, who are responsible for the accuracy of data presented herein. This research was conducted in the: Laboratory for the Chemistry of Construction Materials (LC^2), Electron-Microscopy (EM) Core and Molecular Instrumentation Center (MIC) at UCLA and the CLAS Goldwater Environmental Laboratory at Arizona State University (ASU). The authors gratefully acknowledge the support that has made these laboratories and their operations possible.

REFERENCES

1. Provis JL, Bernal SA. Geopolymers and related alkali-activated materials. *Annu Rev Mater Res*. 2014;44:299-327.
2. Provis JL, van Deventer JS, eds. *Alkali Activated Materials: State-of-the-Art Report, Report RILEM TC 224-AAM*. Dordrecht: Springer/ RILEM; 2014.
3. van Deventer JSJ, Provis JL, Duxon P, Rees CA, Lukey G. Characterization of geopolymer cements and concretes: structure/property relations and commercial utilization, 12th International Congress on the Chemistry of Cement, Montreal, Canada, 2007.
4. Shi C, Fernández-Jiménez A, Palomo A. New cements for the 21st century: the pursuit of an alternative to Portland cement. *Cem Concr Res*. 2011;41:750-763.
5. Bernal SA, Provis JL. Durability of alkali-activated materials: progress and perspectives. *J Am Ceram Soc*. 2014;97:997-1008.
6. Provis JL. Geopolymers and other alkali activated materials: why, how, and what? *Mater Struct*. 2014;47:11-25.
7. Shi C, Krivenko PV, Roy D. *Alkali-Activated Cements and Concretes*. New York: Taylor & Francis; 2006.
8. L'Hôpital E, Lothenbach B, Kulik DA, Scrivener K. Influence of calcium to silica ratio on aluminium uptake in calcium silicate hydrate. *Cem Concr Res*. 2016;85:111-121.
9. L'Hôpital E, Lothenbach B, Scrivener K, Kulik DA. Alkali uptake in calcium alumina silicate hydrate (C-A-S-H). *Cem Concr Res*. 2016;85:122-136.
10. Lothenbach B, Scrivener K, Hooton RD. Supplementary cementitious materials. *Cem Concr Res*. 2011;41:1244-1256.
11. Richardson IG, Groves GW. Microstructure and microanalysis of hardened cement pastes involving ground granulated blast-furnace slag. *J Mater Sci*. 1992;27:6204-6212.
12. Myers RJ, Bernal SA, Provis JL. A thermodynamic model for C-(N-)A-S-H gel: CNASH_ss. Derivation and validation. *Cem Concr Res*. 2014;66:27-47.
13. Saito F, Mi G, Hanoda H. Mechanochemical synthesis of hydrated calcium silicates by room temperature grinding. *Solid State Ion*. 1997;101–103:37-43.
14. Matsuyama H, Young JF. Effects of pH on precipitation of quasi-crystalline calcium silicate hydrate in aqueous solution. *Adv Cem Res*. 2000;12:29-33.
15. Goto S, Akazawa K, Daimon M. Solubility of silica-alumina gels in different pH solutions-discussion on the hydration of slags and fly ashes in cement. *Cem Concr Res*. 1992;22:216-223.
16. Nelson EB. Effect of Na_2O on calcium silicate hydrate at elevated temperatures. *Cem Concr Res*. 1977;7:687-694.
17. Blakeman EA, Gard JA, Ramsay CG, Taylor HFW. Studies on the system sodium oxide–calcium oxide–silica-water. *J Appl Chem Biotechnol*. 1974;24:239-245.
18. Hong SY, Glasser FP. Alkali binding in cement phases. Part I. the C–S–H phase. *Cem Concr Res*. 1999;29:1893-1903.
19. Fernandez-Jimenez R, Wallepu R, Terai T, Palomo A, Ikeda K. Synthesis and thermal behaviour of different aluminosilicate. *J Non-Cryst Solids*. 2006;352:2061-2066.

20. Barbosa VFF, MacKenzei KJD. Synthesis and thermal behavior of a potassium silicate geopolymers. *Mater Lett*. 2003;57:1477-1482.
21. Garcia-Lodeiro I, Fernandez-Jimenez A, Blanco MT, Palomo A. FTIR study of the sol-gel synthesis of cementitious gels: C–S–H and N–A–S–H. *J Sol Gel Sci Technol*. 2008;45:63-72.
22. Richardson IG. The calcium silicate hydrates. *Cem Concr Res*. 2008;38:137-158.
23. Richardson IG, Groves GW. Models for the composition and structure of calcium silicate hydrate (C-S-H) gel in hardened tricalcium silicate pastes. *Cem Concr Res*. 1992;22:1001-1010.
24. Loewenstein W. The distribution of aluminum in the tetrahedra of silicates and aluminates. *Am Mineral*. 1954;39:92-96.
25. Garcia-Lodeiro I, Fernandez-Jimenez A, Palomo A, Macphee DE. Effect of calcium additions on N–A–S–H cementitious gels. *J Am Ceram Soc*. 2010;93:1934-1940.
26. García-Lodeiro I. Compatibilidad de geles cementantes, estudio en muestras reales y polvos sintéticos (in Spanish), Instituto Eduardo Torroja, PhD Thesis, Universidad Autónoma de Madrid, 2010.
27. Myers RJ, Bernal SA, San Nicolas R, Provis JL. Generalized structural description of calcium-sodium aluminosilicate hydrate gels the cross-linked substituted tobermorite model. *Langmuir*. 2013;29:5294-5306.
28. Chen JJ, Thomas JJ, Taylor HFW, Jennings HM. Solubility and structure of calcium silicate hydrate. *Cem Concr Res*. 2004;34:1499-1519.
29. García Lodeiro I, Fernández-Jimenez A, Palomo A, Macphee DE. Effect on fresh C-S-H gels of the simultaneous addition of alkali and aluminum. *Cem Concr Res*. 2010;40:27-32
30. Downs RT, Hall-Wallace M. The American mineralogist crystal structure database. *Am Mineral*. 2003;88:247-250.
31. Famy C, Brough AR, Taylor HFW. The C-S-H gel of Portland cement mortars: Part I. The interpretation of energy-dispersive X-ray microanalyses from scanning electron microscopy, with some observations on C-S-H, AFm and AFt phase compositions. *Cem Concr Res*. 2003;33:1389-1398.
32. Gomez-Zamorano LY, Escalante-García JI. Effect of curing temperature on the nonevaporable water in portland cement blended with geothermal silica waste. *Cem Concr Compos*. 2010;32:603-610.
33. Nocún-Wczelick W. Effect of Na and Al on the phase composition and morphology of autoclaved calcium silicates hydrates. *Cem Concr Res*. 1999;29:1759-1767.
34. Kumar A, Sant G, Patapy C, Gianocca C, Scrivener KL. The influence of sodium and potassium hydroxide on alite hydration: experiments and simulations. *Cem Concr Res*. 2012;42:1513-1523.
35. Macphee DE, Luke K, Glasser FP, Lachowski EE. Solubility and aging of calcium silicate hydrates in alkaline solutions at 25°C. *J Am Ceram Soc*. 1989;72:646-654.
36. Taylor HFW. Nanostructure of C-S-H: current status. *Adv Cem Based Mater*. 1993;1:38-46.
37. Hong SY, Glasser FP. Alkali sorption by C-S-H and CASH gels. Part II. Role of alumina. *Cem Concr Res*. 2002;32:101-1111.
38. Malolepszy J., Alkali activated cementitous materials setting and hardening, *Proceedings of the 3rd International Congress on the Chemistry of Cement*, Beijing, China, 1993
39. Fernández-Jiménez A, Palomo A. Nanostructure/Microstructure of Fly Ash Geopolymers. In: Provis JL, Van Deventer JSJ, eds. *Geopolymers Structure, Processing, Properties and Industrial Applications*. Cambridge, UK: Woodhead Publishing Limited; 2009: 96-113.
40. Fernández-Jiménez A, Palomo A, Sobrados I, Sanz J. The role played by the reactive alumina content in the alkaline activation of fly ashes. *Microporous Mesoporous Mater*. 2006;91:111-119.
41. Criado M, Fernández-Jiménez A, de la Torre AG, Aranda MAG, Palomo A. An XRD study of the effect of the SiO_2/Na_2O ratio on the alkali activation of fly ash. *Cem Concr Res*. 2007;37:671-679.
42. Villa C, Pecina ET, Torres R, Gómez L. Geopolymer synthesis using alkaline activation of natural zeolite. *Constr Build Mater*. 2010;24:2084-2090.
43. Taylor HFW. *Cement Chemistry*, 2nd edn, London, UK: Thomas Telford, 1997.
44. Alizadeh R. PhD Thesis: Nanoestructure and Engineering Properties of Basic and Modified Calcium-Silicate-Hydrate System, Canada, 2009.
45. Blanc P, Bourbon X, Lassin A, Gaucher EC. Chemical model for cement-based materials: temperature dependence of thermodynamic functions for nanocrystalline and crystalline C-S–H phases. *Cem Concr Res*. 2010;40:851-866.
46. Brown PW. The system Na_2O-CaO-SiO_2-H_2O. *J Am Ceram Soc*. 1990;73:3457-3461.
47. Walker CS, Sutou S, Oda C, Mihara M, Honda A. Calcium silicate hydrate (C-S-H) gel solubility data and a discrete solid phase model at 25°C based on two binary non-ideal solid solutions. *Cem Concr Res*. 2016;79:1-30.
48. Glasser FP, Lachowski EE, Macphee DE. Compositional model for calcium silicate hydrate (C-S-H) gels, their solubilities, and free energies of formation. *J Am Ceram Soc*. 1987;70:481-485.
49. Glasser FP, Tyrer M, Quillin K, et al. The chemistry of blended cements and backfills intended for use in radioactive waste disposal, Research and Development Technical Report P98, UK Environment Agency, 1998.
50. Sefcik J, McCormick AV. What is the solubility of zeolite A? *Microporous Mater*. 1997;10:173-179.
51. Kulik DA, Wagner T, Dmytrieva SV, et al. GEM-selektor geochemical modeling package: revised algorithm and GEMS3K numerical kernel for coupled simulation codes. *Comput Geosci*. 2013;17:1-24.
52. Shock EL, Sassani DC, Willis M, Sverjensky D. Inorganic species in geologic fluids: correlations among standard molal thermodynamic properties of aqueous ions and hydroxide complexes. *Geochim Cosmochim Acta*. 1997;61:907-950.
53. Hummel W, Berner U, Curti E, Pearson FJ, Thönen T. *Nagra/PSI Chemical Thermodynamic Data Base 01/01*. Parkland, FL: Universal Publishers, 2002.
54. Johnson JW, Ölkers EH, Helgeson HC. SUPCRT92: A software package for calculating the standard molal thermodynamic properties of minerals, gases, aqueous species, and reactions from 1 to 5000 bar and 0 to 1000°C. *Comput Geosci*. 1992;18:899-947.
55. Myers RJ, L'Hôpital E, Provis JL, Lothenbach B. Composition–solubility–structure relationships in calcium (alkali) aluminosilicate hydrate (C-(N, K-)A-S-H). *Dalton Trans*. 2015;44:13530-13544.
56. Damidot D, Lothenbach B, Herfort D, Glasser FP. Thermodynamics of cement science. *Cem Concr Res*. 2011;41:679-695.

57. Balonis M, Lothenbach B, Le Saout G, Glasser FP. Impact of chloride on the mineralogy of hydrated Portland cement systems. *Cem Concr Res*. 2010;40:1009-1022.
58. Lothenbach B, Winnefeld F. Thermodynamic modelling of the hydration of Portland cement. *Cem Concr Res*. 2006;36:209-226.
59. Matschei T, Lothenbach B, Glasser FP. Thermodynamic properties of Portland cement hydrates in the system CaO–Al_2O_3–SiO_2–$CaSO_4$–$CaCO_3$–H_2O. *Cem Concr Res*. 2007;37:1379-1410.
60. Kulik DA, Kersten M. Aqueous solubility diagrams for cementitious waste stabilization systems: II, end-member stoichiometries of ideal calcium silicate hydrate solid solutions. *J Am Ceram Soc*. 2001;84:3017-3026.
61. Haas J, Nonat A. From C–S–H to C–A–S–H: experimental study and thermodynamic modelling. *Cem Concr Res*. 2015;68:124-138.

SUPPORTING INFORMATION

Additional Supporting Information may be found online in the supporting information tab for this article.

How to cite this article: Gomez-Zamorano L, Balonis M, Erdemli B, Neithalath N, Sant G. C–(N)–S–H and N–A–S–H gels: Compositions and solubility data at 25°C and 50°C. *J Am Ceram Soc*. 2017;100:2700–2711.